

To be published in the Astronomical Journal, June 1999

Using Hubble Space Telescope Imaging of Nuclear Dust Morphology to Rule Out Bars Fueling Seyfert Nuclei¹

Michael W. Regan^{2,3}

Carnegie Institution of Washington, Department of Terrestrial Magnetism,
5241 Broad Branch Road, Washington, DC 20015

John S. Mulchaey⁴

The Observatories of the Carnegie Institution of Washington,
813 Santa Barbara Street,
Pasadena, CA 91101

ABSTRACT

If AGN are powered by the accretion of matter onto massive black holes, how does the gas in the host galaxy lose the required angular momentum to approach the black hole? Gas easily transfers angular momentum to stars in strong bars, making them likely candidates. Although ground-based searches for bars in active galaxies using both optical and near infrared surface brightness have not found any excess of bars relative to quiescent galaxies, the searches have not been able to rule out small-scale nuclear bars. To look for these nuclear bars we use HST WFPC2-NICMOS color maps to search for the straight dust lane signature of strong bars. Of the twelve Seyfert galaxies in our sample, only three have dust lanes consistent with a strong nuclear bar. Therefore, strong nuclear bars cannot be the primary fueling mechanism for Seyfert nuclei. We do find that a majority of the galaxies show an spiral morphology in their dust lanes. These spiral arms may be a possible fueling mechanism.

Subject headings: galaxies: Seyfert — galaxies: ISM — galaxies: nuclei

¹Based on observations with the NASA/ESA Hubble Space Telescope, obtained at the Space Telescope Science Institute, which is operated by the Association of Universities for Research in Astronomy, Inc. under NASA contract No. NAS5-26555

²Email-mregan@dtm.ciw.edu

³Hubble Fellow

⁴Email-mulchaey@ociw.edu

1. Introduction

One of the goals of AGN research is to try to understand what transports the gas from the large host galaxy scales ($\sim 1\text{-}10\text{ kpc}$) down close enough to the nucleus ($< 1\text{ pc}$) to fuel an AGN. To accomplish this fueling the gas must decrease its angular momentum by several orders of magnitude. How does the gas lose its angular momentum? One possibility is that gas could lose angular momentum to stars in the shocks and gravitational torques caused by a bar-like gravitational potential (Sholsman, Frank, & Begelman 1989). If this is true, we might expect there to be more bars in active galaxies than in quiescent galaxies. Surveys have looked for this excess of bars and none has been found (Kotilainen et al. 1992; Zitelli et al. 1993; McLeod & Reike 1995; Alonso-Herrero, Ward, & Kotilainen 1996; Mulchaey & Regan 1997; Ho, Filippenko, & Sargent 1997). The lack of observational evidence for an excess of bars in these survey has not ruled out bars as a mechanism of fueling active galaxies for several reasons. One possibility is that there is an inherent difference between active galaxies and normal galaxies in that not all normal galaxies may contain a massive black hole. In this case the lack of an excess of bars in Seyfert galaxies compared to normal galaxies would not rule out bars as a fueling mechanism. However, recent studies of quiescent galaxies using both ground-based observations and the HST have revealed kinematic evidence for the presence of black holes in almost every galaxy studied (Kormendy & Richstone 1995). Another possibility is that, due to a lack of resolution, all studies to date have been unable to detect small scale bars ($< \sim 3''$), which are all that is necessary to provide fuel to an AGN.

Almost all studies of AGN fueling in the past have focused on looking for non-axisymmetric perturbations in the stellar surface density under the assumption that these lead to perturbations in the gravitational potential. However, this may not be the best way to search for small-scale nuclear bars. Even in the near infrared the stellar surface density is subject to contamination by dust extinction and regions of current star formation. This contamination makes it hard to determine the gravitational potential from the stellar surface density. Since the fuel for AGN is provided by the interstellar medium (ISM), another avenue of investigation is to study the ISM directly. Because the ISM in spiral galaxies is dynamically cold, it responds strongly to perturbations in the gravitational potential. If we can characterize the morphology of the ISM, it could provide a more sensitive probe of the gravitational potential than the stellar surface density morphology.

To search for the signatures of a nuclear bar using the ISM morphology requires the resolution of the Hubble Space Telescope (HST). In this paper we present our observations of Seyfert galaxies made with the Near Infrared Camera and Multi-object Spectrometer (NICMOS). We combine the NICMOS observations with archival observations of the same

galaxies made with the Wide Field and Planetary Camera 2 (WFPC2) to form color maps. We use these color maps to investigate the nuclear ISM morphology of a set of Seyfert galaxies as a test of whether small scale bars fuel Seyfert nuclei.

2. Using the ISM as a Probe of the Gravitational Potential

Since stars compose the vast majority of the mass in the central regions of disk galaxies, it would make sense to search for perturbations in the gravitational potential by looking at the stellar surface density. The problem is that the stars in the old stellar disk have velocity dispersions of ~ 40 km s $^{-1}$ (Mihalas & Binney 1981) which will tend to wash out the effects of perturbations. To complicate matters, in the nuclear regions of galaxies the velocity dispersion of the spheroid component is >100 km s $^{-1}$ leading to even more smoothing of the surface density variations. The low velocity dispersion of the ISM (~ 4 km s $^{-1}$ in the local disk of the Milky Way (Combes 1991)) will lead to much larger surface density perturbations, making it a better probe of the gravitational potential. To quantify the advantage of using the ISM surface density, we can compare the surface density variations of the two components using a model galaxy. For our model galaxy we determine the stellar surface density by adding the contributions of three mass components: a disk, a bulge, and a bar. The surface density of the Kuzmin-Toomre disk component, σ_d , is

$$\sigma_d(r) = (v_0^2/2\pi Gr)(1 + r^2/r_0^2)^{-1.5}, \quad (1)$$

where $v_0 = 164$ km s $^{-1}$ and $r_0 = 20$ kpc. The volume density of the bulge, ρ_b , is

$$\rho_b = \rho_{cen}(1 + r^2/r_{core}^2)^{-1.5}, \quad (2)$$

where ρ_{cen} is the central density of the bulge and r_{core} is the core radius of the bulge. We use a Ferrers ellipsoid for the bar density with a density, ρ_{bar} , of

$$\rho_{bar} = \rho_0(1 - g^2) \quad \text{for } g < 1 \quad (3)$$

and

$$\rho_{bar} = 0 \quad \text{for } g \geq 1,$$

where $g^2 = y^2/a^2 + (x^2 + z^2)/b^2$ and a and b are the semi-major and semi-minor axis, respectively. To convert the volume densities into observable units we integrate the volume densities of the bar and bulge over ± 10 kpc in the z direction to form surface densities. We then sum the three surface density components to give the total surface density (Figure 1a).

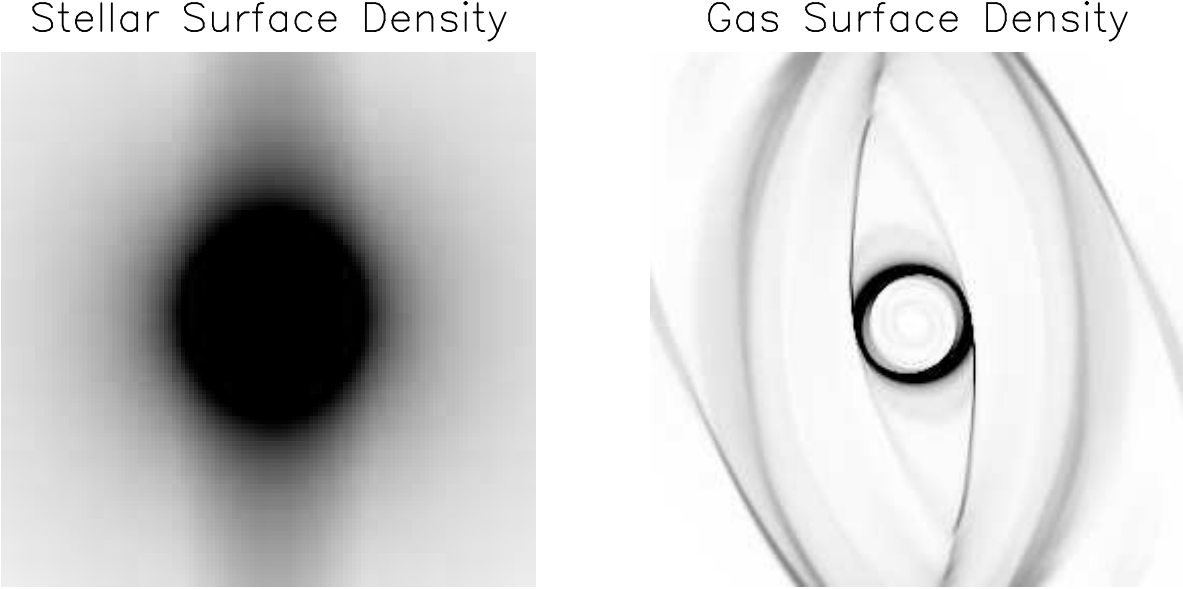


Fig. 1.— a) The model stellar surface density of barred galaxy. b) The model gas surface density of a barred galaxy. Notice how the dust lanes along the leading edge of the bar are straight. This is the signature of a strongly barred galaxy.

We use the hydrodynamic models of gas flow in a barred potential from Piner, Stone & Teuben (1995) to find the gas surface density for this mass surface density. The resulting gas surface density is shown in Figure 1b. The peak variation in the azimuthal gas surface density occurs at a radius of ~ 2 kpc. At this radius the azimuthal gas surface density variation is ~ 20 to 1. At that same radius in the stellar surface density (Figure 1a) the peak density variation with azimuth is ~ 2.2 to 1. Therefore, at a given level of sensitivity to azimuthal surface density variations, the ISM surface density will reveal much smaller non-axisymmetric perturbations than the stellar surface density.

Detecting the ISM surface density variations at sub-arcsecond resolution cannot be done with conventional methods of observing the ISM in galaxies such as millimeter interferometers and thermal infrared observations of dust. Although the current generation of millimeter arrays do have sub-arcsecond resolution, they will not have the surface brightness sensitivity to detect normal molecular clouds at this resolution until the arrival of the Millimeter Array. Thermal infrared observations by ISO of hot dust in Centaurs A did reveal a the expected dust morphology of a strong bar (Mirabel et al. 1999) but the resolution of these observations was $3''$ which will only resolve the dust morphology in relatively nearby galaxies. An alternative method for observing the morphology of the ISM, is to look for the dust component of the ISM in extinction. One problem with using

dust extinction as a tracer of the ISM is that if the extinction is high enough for the dust to become optically thick then the light will be dominated by the foreground unreddened stars. This leads to regions with large amounts of dust having relatively unreddened colors. This problem can be minimized by using a near infrared color as the long wavelength color, which will provide a much larger dynamic range of dust column depths that will be detectable in an extinction map.

Another advantage of using the dust morphology to probe the potential instead of the stellar surface density is that the problem of the stellar isophotes being influenced by the presence of dust or regions of current star formation is avoided. This effect can even be significant in the near infrared where the extinction due to dust is much lower than in the optical. A foreground dust feature with an optical extinction of $A_v=2$ leads to a 25% reduction in the transmitted light at $1.6\mu\text{m}$. Stronger dust features are common in our color maps (see Figure 2) which will lead to biases if near infrared isophotes alone are used. Biases will also be induced by regions of current star formation that are not obvious in the NICMOS images alone.

Figure 1b shows that the dust morphology of a barred galaxy has a very specific signature which can be used to infer the presence of a bar. The dust lanes along the leading edge of the bar are always very straight in strongly barred galaxies (Athanassoula 1992; Piner et al. 1995). It is these strong bars that are proposed to drive gas inward since in less strongly barred galaxies there may not be a shock in the dust lanes (A92). In galaxies with weaker bars, the dust lanes along the leading edge of the bar are curved, with the degree of curvature increasing as the bar weakens. In general, it is hard to distinguish the dust morphology of a weak bar from the dust morphology of high pitch angle spiral arms (Regan & Vogel 1994).

These simple models suggest that the dust morphology of a galaxy can be a sensitive probe of its gravitational potential. By searching for straight dust lanes we can determine if galaxies have strong bars that are depriving the gas of angular momentum and thus driving it inward. Since we are directly probing the fuel of the AGN we are less prone to biases caused by dust and star formation.

3. Observations and Data Reduction

Observations were made using the F160W filter on camera 2 of the Near Infrared Camera and Multi-Object Spectrometer (NICMOS) in the Hubble Space Telescope from the dates of 17 June 1997 to 18 March 1998. The twelve galaxies in this sample are a

subset of our larger NICMOS sample of active and quiescent galaxies. These objects are the first twelve in our sample observed by NICMOS for which HST observations at optical wavelengths were available in the archive. The F160W filter is an approximate match to ground-based near infrared H-band filters and has a central wavelength of $1.6\mu\text{m}$. Our total integration time on source was either 704 or 640 seconds. The shorter integration times were for those galaxies where we dithered the telescope to allow for the removal of bad pixels. The detector on Camera 2 is a 256×256 HgCdTe detector with a plate scale of 0.075 arc seconds pixel^{-1} yielding a field of view of $19''.2$. During the time period of the observations the pipeline data reduction for NICMOS was still under development leading to output of the pipeline process that was not the best possible calibration of the data. Therefore, we recalibrated the images using the latest flat fields, darks, and non-linearity files. The NICMOS images are shown in Figure 2.

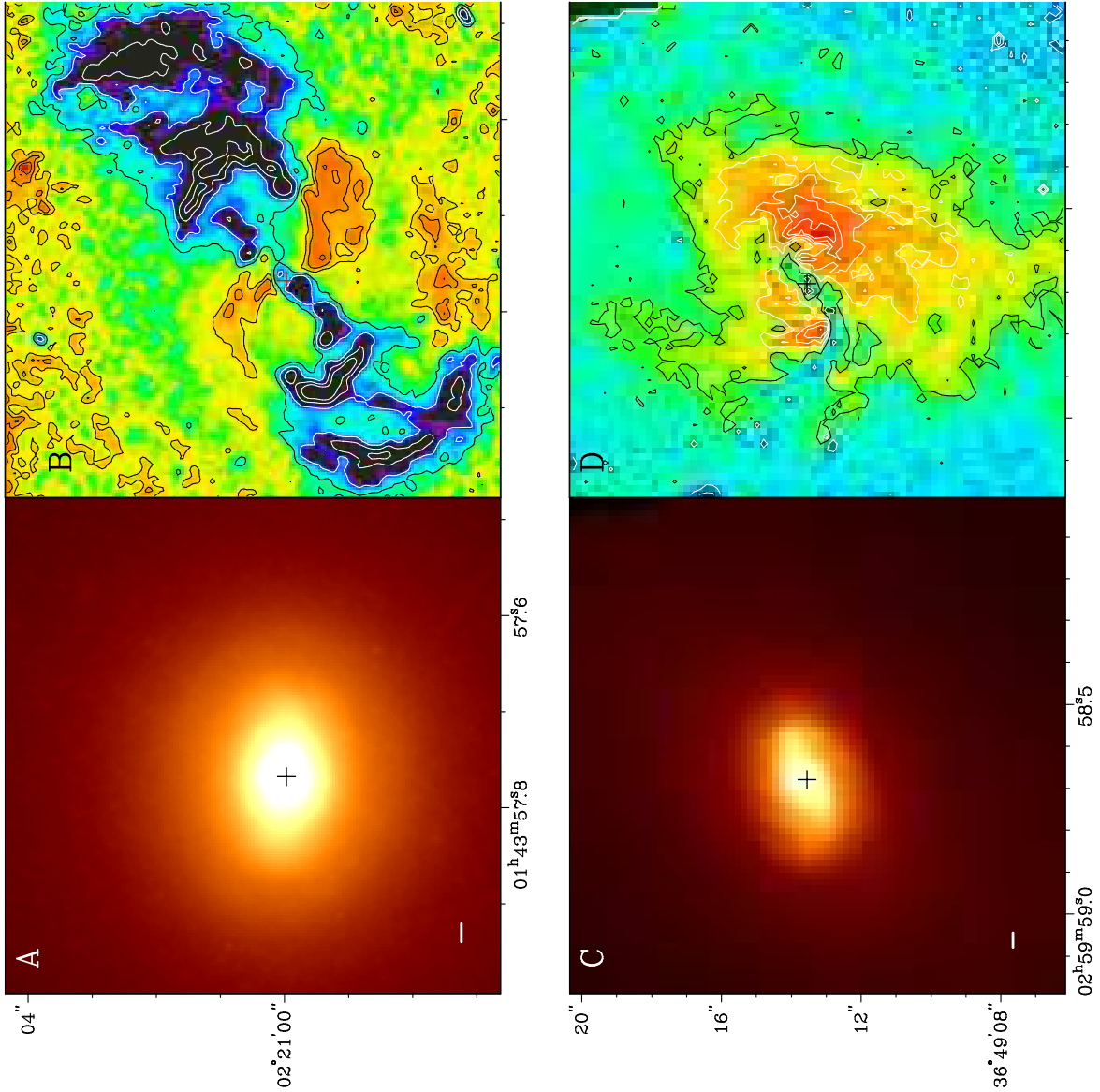
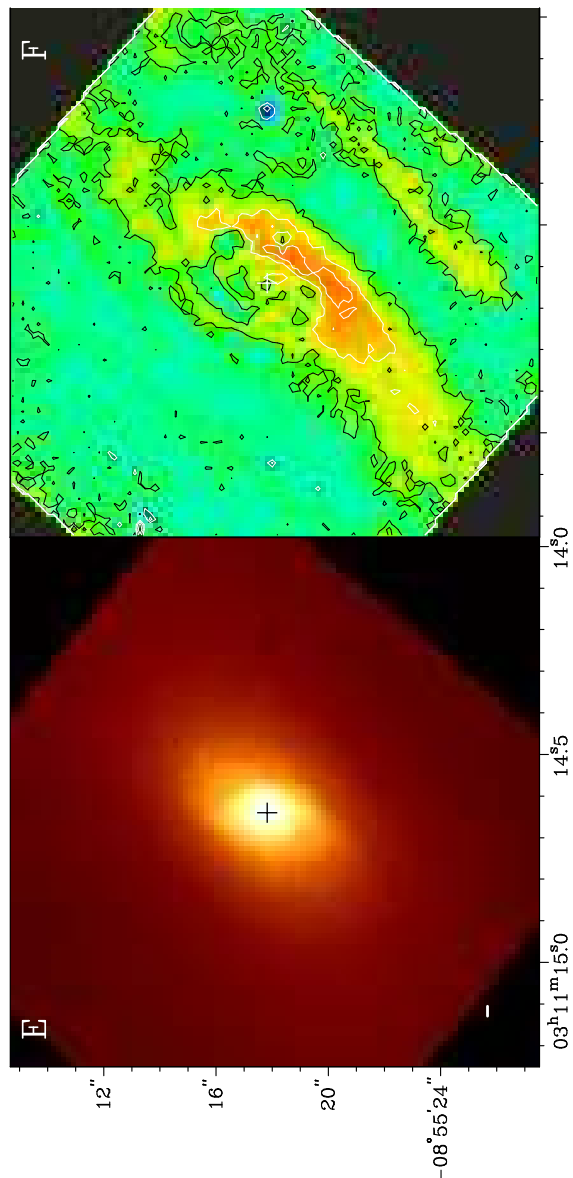
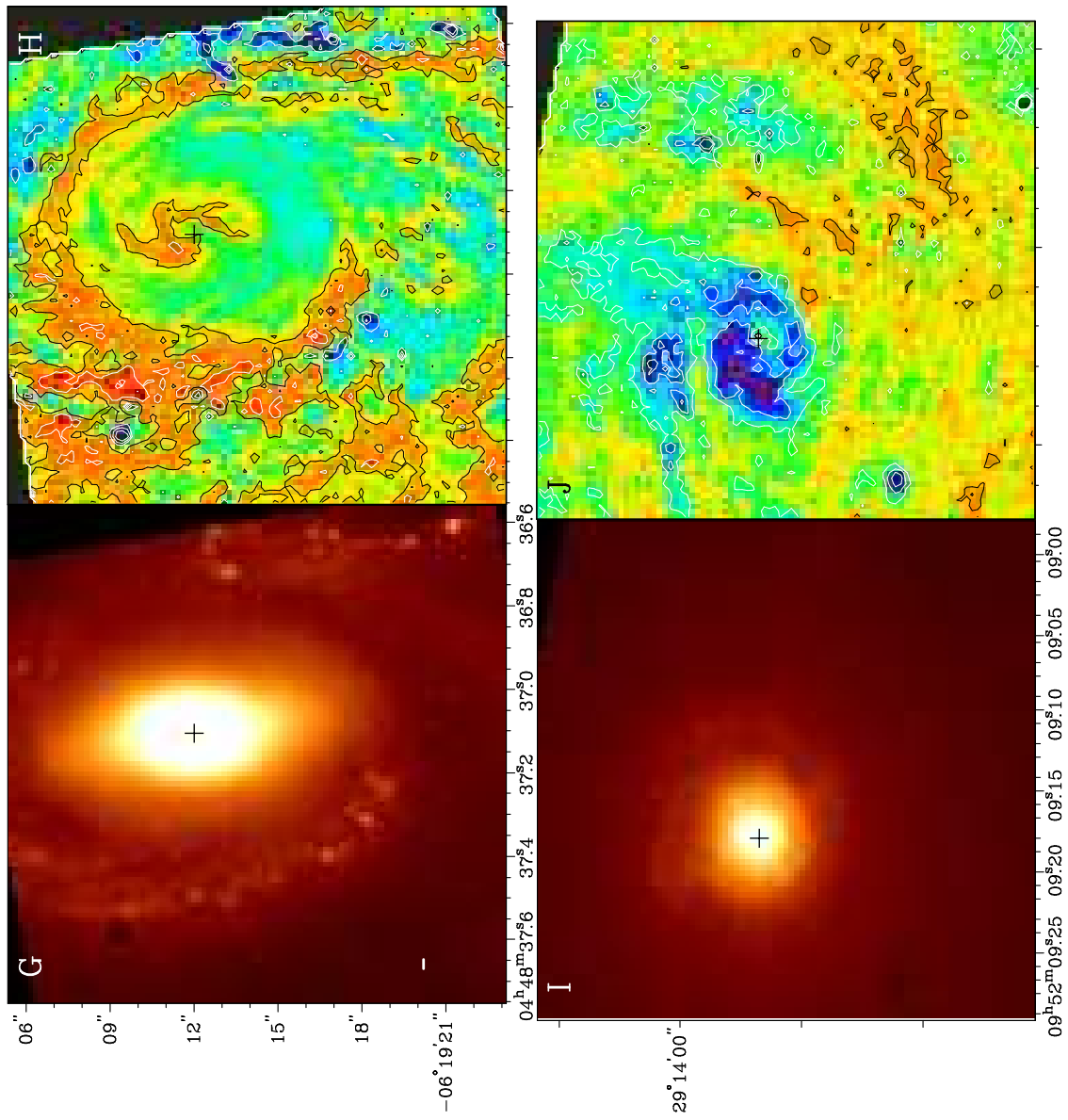
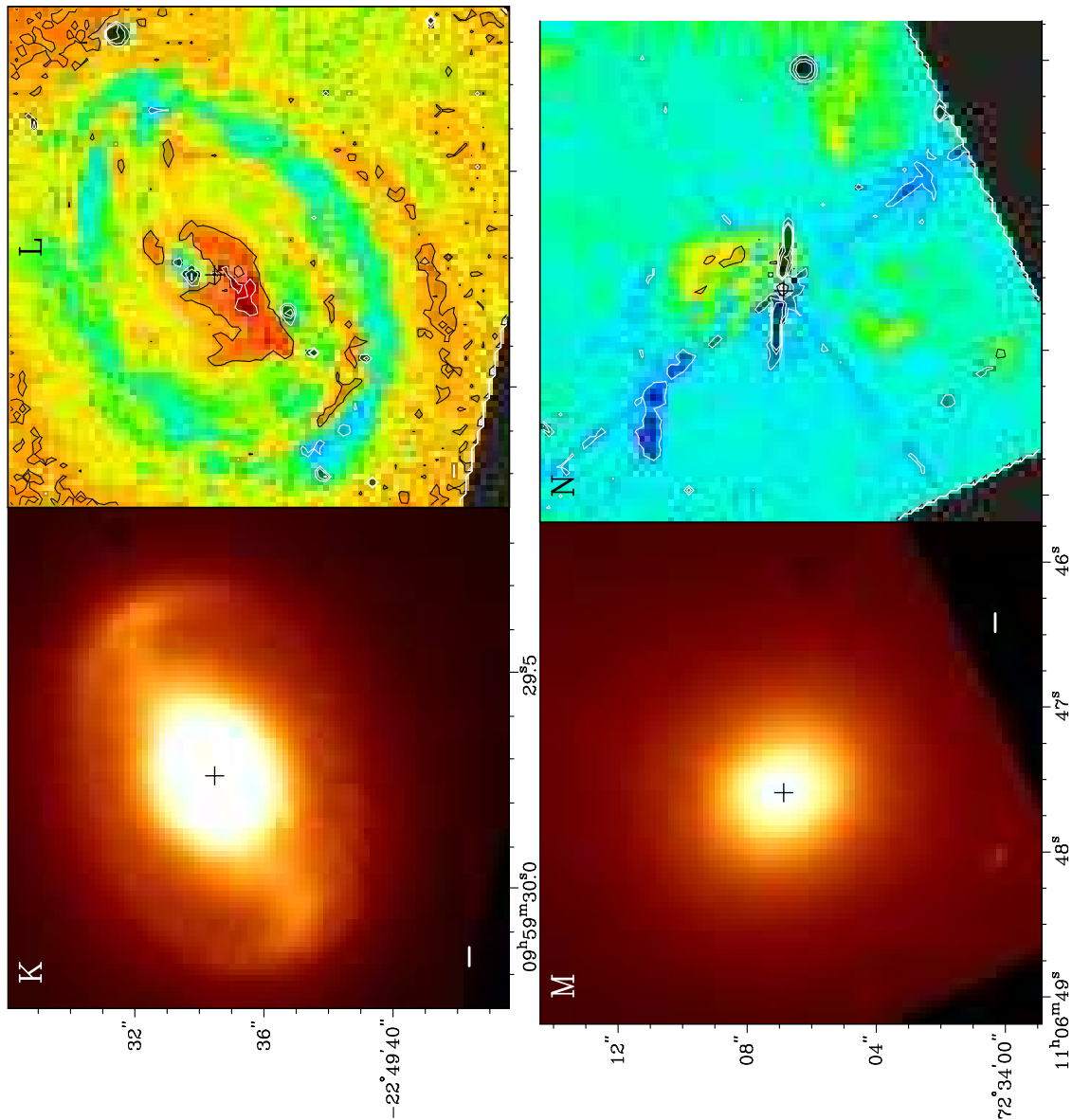
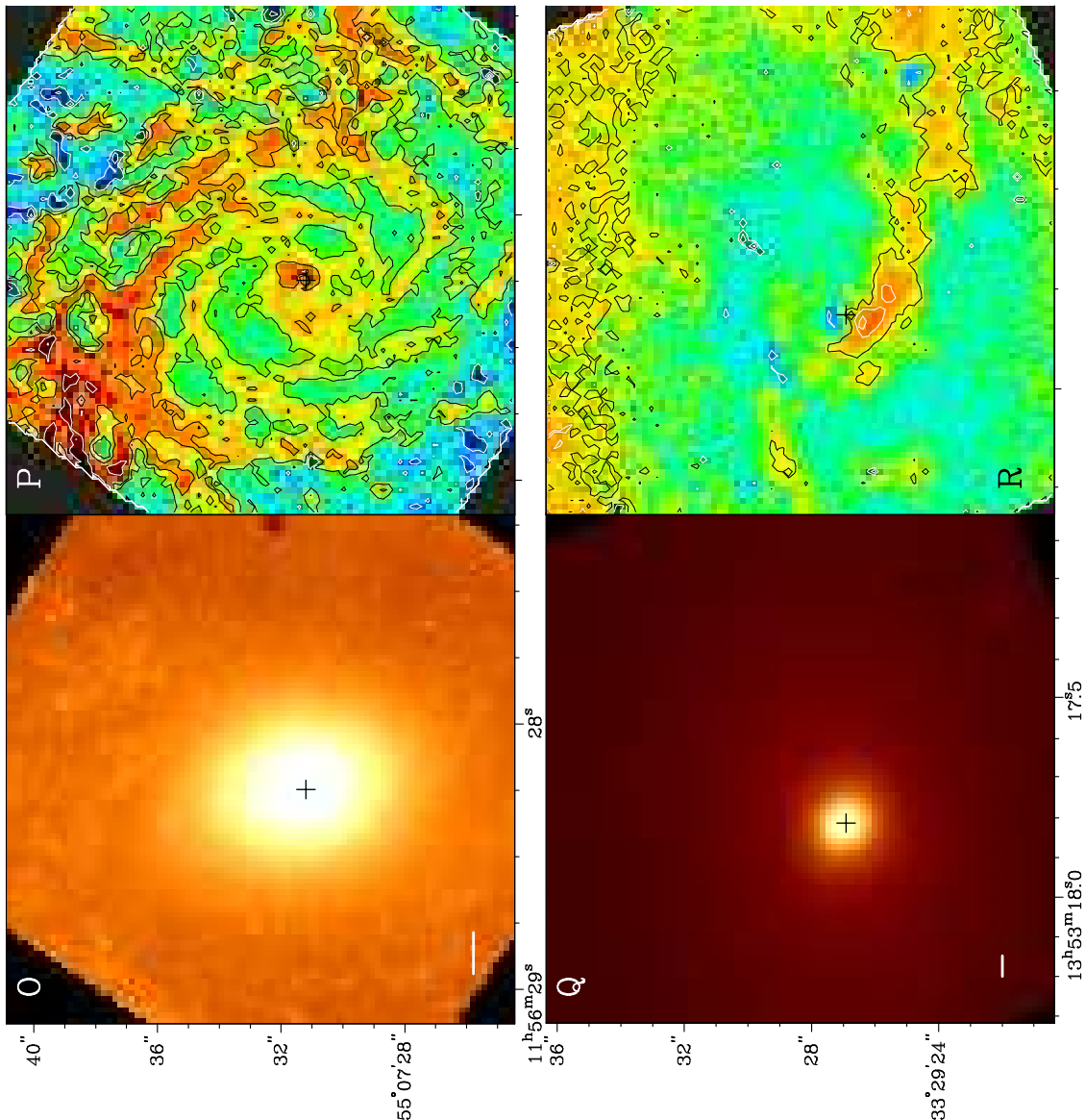


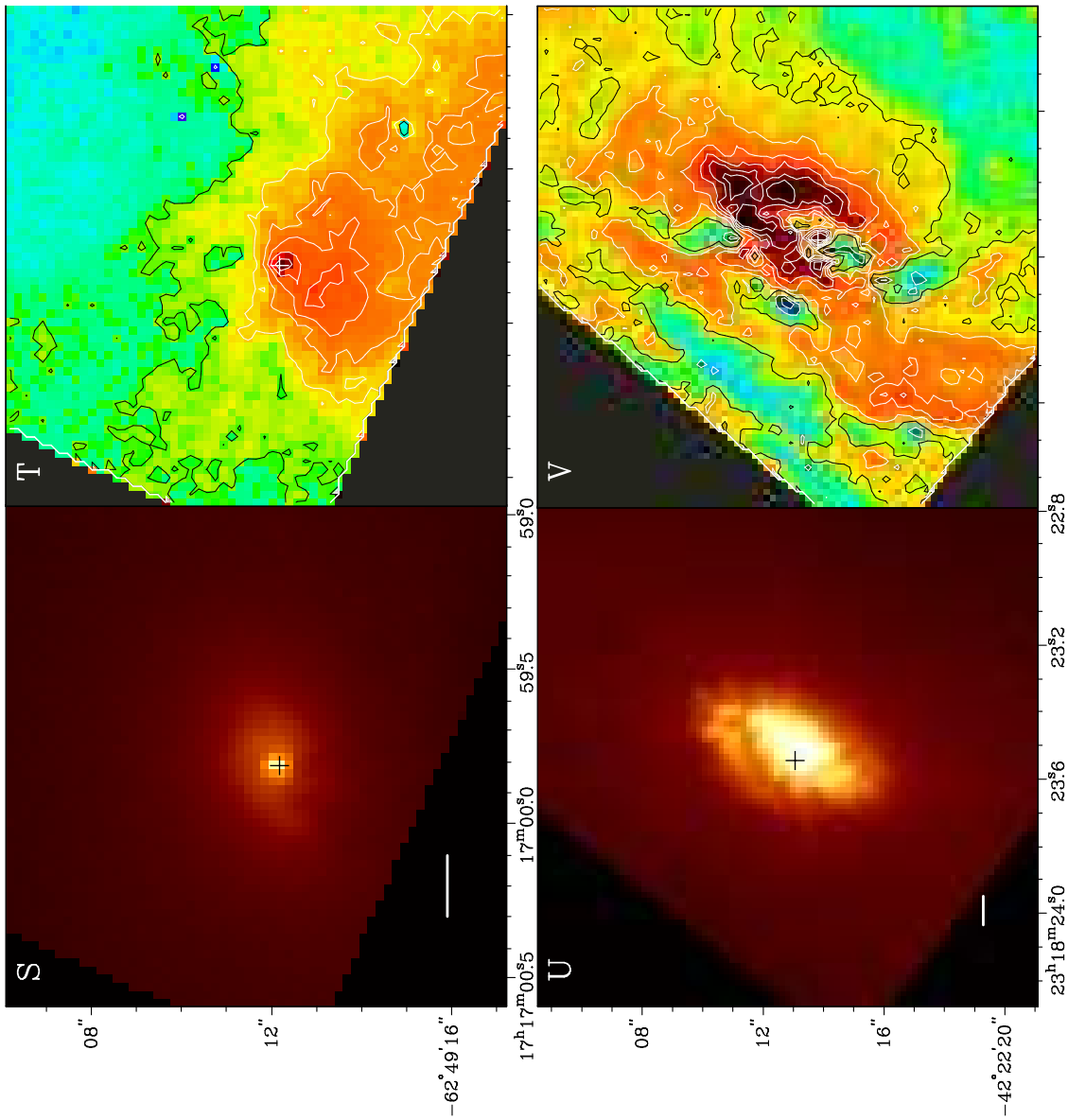
Fig. 2.— Near infrared NICMOS $1.6\mu\text{m}$ and color maps for the sample galaxies. Left column - NICMOS image taken at $1.6\mu\text{m}$ using the F160W filter; the cross marks the peak of the emission. The white bar in the lower left corner shows a linear scale of 100pc assuming $H_0=75 \text{ km s}^{-1} \text{ Mpc}^{-1}$. Right column - color map made by combining the NICMOS $1.6\mu\text{m}$ image with a WFPC2 F606W Image. The contours represent the red and blue color excesses compared to the background galaxy. The contours of F606W–F160W blue color excess are at -0.2, -0.5, and -0.8. The contours of F606W–F160W red color excess are at 0.3, 0.6, 0.9, 1.2, 1.5, and 1.9 magnitudes. ab) Mkn 573 cd) Mkn 1066 ef) NGC 1241 gh) NGC 1667 ij) NGC 3032 kl) NGC 3081 mn) 3516 op) NGC 3982 qr) NGC 5347 st) NGC 6300 uv) NGC 7582 wx) NGC 7743

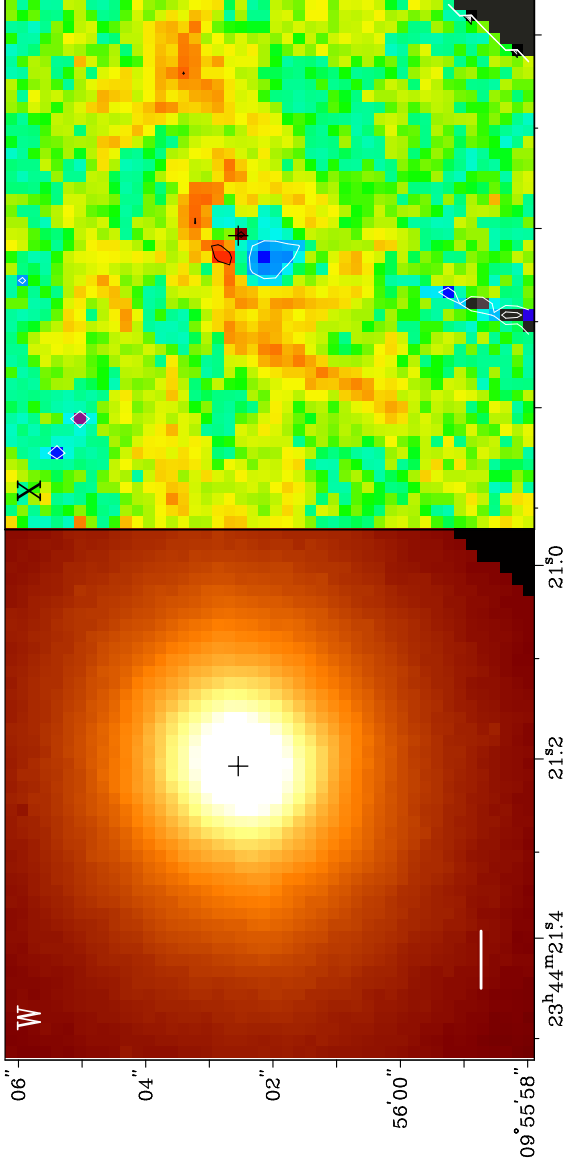












We obtained optical images of the galaxies from the Hubble Data Archive. These images were taken using the F606W filter using 500 second exposures with the Wide Field and Planetary Camera 2 and have previously been published by Malkan, Gorjian, & Tam (1998). Since we were only interested in the regions that overlapped our NICMOS images, we only used the planetary camera (PC) images. We registered the NICMOS images to match the orientation and plate scale of the PC images. After registration there still was a 1-2" offset between the NICMOS and PC images. Therefore, we then performed a final shift to align the nucleus in the two images. We then smoothed the PC images to same resolution as the NICMOS images and divided the PC images by the NICMOS images to

form color maps. To make comparisons of extinction features in galaxies we need to know the color of the underlying stellar population. For all the galaxies, except NGC 3982, we set the color excess to be zero when the ratio of the count rate in the PC image to the count rate in the NICMOS image was 0.09. The underlying population in NGC 3982 is bluer than the other galaxies leading us to set the color excess for this galaxy to zero when the ratio of the count rates was 0.11. The color maps for each of the sample galaxies are shown in Figure 2.

4. Results

4.1. Individual Galaxies

4.1.1. *Markarian 573*

The is a well studied Seyfert 2 galaxy with two ionization cones (Falcke, Wilson, & Simpson 1998; Pogge & De Robertis 1995). The color map shows both blue color excess (light colors) and red color excess (dark colors) regions. The region of the blue excess is delimited by two cones but there is interesting structure within the blue regions. Since the position angle of the cones in our color map (123°) agrees well with the ground based ionization cone position angle (124° (Pogge & De Robertis 1995)) the ionization cone is the blue feature in our color map. The excess emission in the F606W filter within the ionization cone is likely due to $\text{H}\alpha$ emission included in the F606W filter bandpass.

What is unusual about this galaxy is that the red absorption features connect to the blue emission features. The strong red feature to the south of the nucleus can be seen to directly connect to the very blue feature $2''$ west of the nucleus. The weaker red dust lane to the north of the nucleus connects to both a strong blue feature $0''.75$ northwest of the nucleus and faintly to the strong ridge of blue emission $2''$ east of the nucleus. The two fainter outer red features can also be seen to connect to the blue feature. The red feature $3''$ to the southeast of the nucleus connects to the outer blue ridge with then shows a faint connection to a red feature to the northeast of the nucleus. The broad red feature just to the southeast of the nucleus shows a faint connection to the broad blue feature east of the nucleus. A possible reason for the connection between the features is that the blue features are dust lanes illuminated from a central ionizing source.

Given the connection between the two types of features we can see that Markarian 573 has four symmetrical spiral dust lanes. Each dust lane traces about 180 degrees of arc as it spirals into the central region. The two outer dust lanes seem to have a higher pitch angle

since they reach the same radius as the two inner arms over the same angular extent even though they start at about twice the radius of the inner arms.

4.1.2. *Markarian 1066*

The NICMOS image (Fig. 2C) reveals what at first glance appears to be a nuclear bar with a position angle of $\sim 135^\circ$. But our color map (Fig. 2D) shows that the extension is caused by the regions of current star formation just northwest and southeast of the nucleus. The large amount of dust in this galaxy is quite evident as is the overall spiral pattern to the dust. A single broad dust lane seems to dominate the morphology. This dust lane approaches the nucleus from the southeast and reaches a maximum extinction about $1''$ west of the nucleus. A less well defined arm approaches the nucleus from the north and reaches a maximum reddening about $1''$ east of the nucleus. Just south of the maximum reddening the colors quickly change to blue. It is clear from the figure that the dust is in a highly non-axisymmetric distribution since the majority of the extinction is seen to the southwest of the nucleus.

A string of blue features are seen east of the nucleus starting about $1''.5$ east of the nucleus and approach as close as $0''.5$ to the nucleus. They seem to connect to two blue features that are just east and west of the maximum reddening of the western dust lane about $1''$ west of the nucleus.

4.1.3. *NGC 1241*

The color map for NGC 1241 (Fig. 2F) reveals an overall dust morphology that is consistent with an inclined ring at the terminus of bar dust lanes. There is a red half ellipse close to the nucleus with a minor axis of about $1''.5$ and a major axis of $\sim 4''$. The other side of the ellipse does show in extinction but at a much lower level. This ellipse connects to red features that lead off the image to the southeast and northwest. The overall reddening to the southwest of the nucleus is stronger implying that this is the near side of the galaxy.

4.1.4. *NGC 1667*

The HST color map of NGC 1667 (Fig. 2H) reveals a complex but relatively ordered dust morphology with a nuclear spiral morphology. The overall extinction is stronger to the northeast of the nucleus. From the southwest a relatively straight dust lane approaches the

nuclear region until it intersects a nuclear ring. Here it curves around until it joins the opposite dust lane approaching the ring from the north. The ring then continues around until it is south of the nucleus where it then becomes hard to trace. Inside the ring a multi-armed spiral pattern is seen near the nucleus. These two arms are only roughly symmetrical and the center of symmetry does not appear to be the nucleus. Blue, presumably star forming, regions are also visible in the map as clumps to the west of the western dust lane and about 7" southeast of the nucleus near where the eastern dust lane intersects the dust ring.

4.1.5. *NGC 3032*

Overall, NGC 3032 is much redder to the southwest and the nucleus is surrounded by a disk of blue emission in a spiral pattern. In addition, a strong blue emission region is seen 3" northeast of the nucleus. Two red dust lanes can also be seen in the image. The inner dust lane approaches from the north of the nucleus and curves around the western side of the nucleus at a distance of 4" to connect to the blue disk southeast of the nucleus. The other dust lane enters the image from the northwest and then exits the image to the southeast. It may reenter the map northeast of the nucleus where a dust lane appears to connect to blue features north of the nucleus.

4.1.6. *NGC 3081*

NGC 3081 was one of the best examples of a double-barred galaxy in the survey of Mulchaey, Regan & Kundu (1997). The large bar had a radius of 37" while the nuclear bar had a radius of 6". The nuclear bar can be seen in both the NICMOS image (Figure 2K) and the color map (Figure 2L). The most striking feature of the dust morphology is the ring of extinction just outside of the nuclear bar. Outside of this red ring feature in the color map is a more diffuse region of blue colors. Both the red and blue features are stronger to the southwest of the nucleus. A ring of star formation seen just outside of a bar is a common feature and has been termed an inner ring (Buta 1986). At the ends of the bar we can see faint regions of enhanced star formation 6" from the nucleus to the southeast and to the northwest.

Within the nuclear bar along the leading edges of the bar there is a relatively wide and dense region of extinction to the southeast. On the other hand, the northwestern bar half shows much less extinction. It does have a very blue, probably star forming, region just

north of the nucleus. The small separation of the star forming region from the active nucleus ($\sim 1''$ or 160 pc) has probably caused confusion in ground based images and spectra of this galaxy.

4.1.7. *NGC 3516*

A single spiral dust pattern dominates the morphology of the S0 galaxy, NGC 3516. The main red dust lane emerges from the blue feature north of the nucleus at a radius of $\sim 3''$. It then appears to spiral around the nucleus and get closer until it is lost in the diffraction effects $\sim 0''.5$ from the nucleus. The extinction in the map is very asymmetric with the majority being concentrated in north of the nucleus. The saturated nucleus in the WFPC2 image creates several artifacts in the color map. These are the blue cross and the very blue east-west ridge. A fainter red linear feature to the North and South is due to the diffraction spikes in the NICMOS image.

There seems to be a connection between the dust lane to the north of the nucleus seen in extinction and a blue feature to the northeast of the nucleus. The morphology of the blue feature is not consistent with it arising from star formation since it shows a filamentary structure. The blue emission to the southwest of the nucleus also is more extended than the diffraction spikes. The diffuse blue emission $\sim 1''.5$ southwest of the nucleus appears to connect to the red excess seen $5''$ west southwest of the nucleus.

4.1.8. *NGC 3982*

The global extinction morphology of NGC 3982 is clearly a spiral pattern with more extinction to the north of the nucleus (Fig. 2P). The spiral pattern appears to be multi-armed with there being between two and four arms depending on how they are identified. One spiral arm can be traced over 360° degrees of arc and approaches to within the resolution of our images ($0.15''$ or 10 pc). Blue features are visible to the $\sim 8''$ southeast and northwest of the nucleus on the outside of the dust lanes. The dust lanes in the images also seem to be quite smooth as they near the nucleus compared to their more clumpy nature toward the outer edge of the images (750 pc from the center).

4.1.9. *NGC 5347*

The main dust feature in the map is the broad slightly curved dust lane that approaches the nucleus from the southwest and spirals around to the east of the nucleus. This is the type of dust lane that a strongly barred potential will create. There is also a blue region just to the north of the nucleus at a distance of $1''$ (160 pc) which seems to connect to the main dust lane. A fainter extinction feature can also be seen to the northeast of the nucleus that connects to north of the nucleus.

4.1.10. *NGC 6300*

The overall morphology of the extinction in NGC 6300 (Fig. 2T) shows no organization except that the extinction is much stronger to the south of the nucleus than to the north with the peak emission being just south of the nucleus.

4.1.11. *NGC 7582*

The dust morphology of NGC 7582 (Fig. 2V) is quite complex in this galaxy but is dominated by a dense ring of extinction. This elliptical ring of extinction with a minor axis of $\sim 2''$ and a major axis of $\sim 3''$ surrounds the nucleus. The ring is broken to the southeast by a chain of blue clumps. The closest of these clumps is $\sim 0''.5$ from the nucleus and the chain extends out to $4''$ from the nucleus. Two other blue clumps can be seen $\sim 3''$ east and $\sim 4''$ north of the nucleus. A broad dust lane enters the image from the southeast and connects to the extinction ring north of the chain of blue clumps. As in Markarian 1066 the NICMOS image alone implies that there may be a nuclear bar but the color map shows that this may be just a combination of extinction and star formation perturbing the $1.6\mu\text{m}$ isophotes.

4.1.12. *NGC 7743*

The dust morphology of NGC 7743 (Fig 2X) is consistent with a barred morphology. The strongest dust lane is fairly straight starting to the southeast of the nucleus but then it curves around the northern side of the nucleus. It is then ends at clump of blue emission $0''.5$ north of the nucleus. Two other fainter dust lanes can also be seen. One south of the nucleus curves around to join the southeastern dust lane east of the nucleus. Another dust

lane seems to start north of the nucleus and curves around to the west and south of the nucleus. A blue region of can be seen 1" southeast of the red nucleus.

5. Discussion

5.1. Overall Dust Morphology

We characterize the nuclear dust morphology of the sample galaxies as barred, spiral, ring-like, or amorphous in Table 2. Dust morphologies consistent with a strong bar are found in only three of the galaxies ruling out strong bar potentials as being the primary fueling mechanism for all Seyfert nuclei. Even so, these observations do not rule out bars as fueling mechanisms for the more luminous active galaxies such as quasars and radio galaxies. A weak bar cannot be ruled out in Mkn 1066 or NGC 3516 where the dust morphology shows spiral arms with high pitch angles. This type of dust morphology could result either from spiral arms or a weak bar.

The other galaxies that exhibit spiral dust lanes (Mkn 573, NGC 1667, NGC 3032, and NGC 3982) cannot have even a weakly barred nuclear potential because they either have a multiple armed pattern or the pattern is tightly wound (low pitch angle). A nuclear spiral pattern has been seen before in many galaxies (NGC 7252 - Whitmore et al. 1993; Miller et al. 1997, NGC 278 - Phillips et al. 1996, NGC 4414 - Thornley & Mundy 1997, NGC 5248 - Laine et al. 1998 and in several Coma cluster galaxies Caldwell, Rose, & Dendy 1997) in both young blue stars and in dust extinction and thus appears to be a common feature in disk galaxies.

In a recent paper on NGC 2207 Elmegreen et al. (1998) discuss acoustic noise as a possible formation mechanism for flocculent nuclear spirals disconnected from the global spiral pattern. This formation mechanism could explain the types of patterns we see in NGC 1667 but it does not seem like it can explain the spiral patterns in all the other galaxies. Most notably in NGC 3982 we see that the nuclear spiral pattern is continuous and connects to the larger scale spiral arms.

The two galaxies with a ring-like morphology (NGC 1241 and NGC 7582) do show dust features that connect from the nucleus to the ring. What makes them different than NGC 1667 or NGC 3081, which also show a ring of dust, is that we cannot distinguish the morphology of the dust interior to the dust rings.

The amorphous morphology of NGC 6300 in many ways is the most interesting. It only takes a small non-axisymmetric perturbation of the potential to induce a strong ordering to

the gas morphology in a very short period of time. Even the weakest bar potentials show a very regular gas morphology (Anthanasoula 1992). If the gas was to have enough mass for self-gravity to be important one would expect that it would be unstable against multiple spiral arm formation (Lin & Shu 1964). If not, then the acoustic noise mechanism might be expected to form a spiral pattern. The lack of structure cannot be explained by a lack of linear resolution, since NGC 6300 is one of the closest galaxies in the sample.

5.2. Dust Content

Although, the reddening that we observe for a given amount of dust is very dependent on the location of the dust relative to the stars (Witt, Thronson, & Capuano 1992), we can still make some estimates of the total amount of dust and even the geometry from the WFPC2-NICMOS color maps. Because a given amount of dust produces the most reddening when the dust is in front of all the stars, we can derive lower limits for the dust column depth using our single color. The amount of reddening that can be produced due to dust absorption is limited, if we make the more realistic assumption that the dust and stars are mixed together. The mixing of the dust and stars causes the stars on the far side of the dust to contribute less light. The reduction in light from the background stars causes the observed colors to be dominated by the unreddened foreground stars. We can easily predict the reddening that will be observed for a given ratio of foreground to background stars, if we make the approximation that the dust scale height is small relative to the scale height of the stars. The reddening that would be observed for a various amounts of dust, based on the dust characteristics of Bruzual, Magris, & Calvet (1988) is shown in Figure 3. The observed reddening is reduced if the dust back-scatters the light from the foreground stars so this Figure gives lower limits to the dust content.

Figure 3 shows that if the dust is in the mid-plane of the galaxy, as we would expect near the nucleus where a large fraction of the stars are in a extended spheroid or bulge, then the maximum color excess we could observe would be ~ 0.6 magnitudes. The maximum extinction found in each of the galaxies is shown in Table 2. In most of the galaxies a significant amount of dust must be above the mid-plane of the stars. In fact, for three galaxies the dust must be in front of over 90% of the stars to account for the observed color excess.

The simplest explanation for the high color excesses is that we are observing a plane of dust inclined with respect to the bulge stars. This would cause the dust on the near side of the bulge to be in front of most of the bulge stars. This projection effect would only apply in regions that are neither too near the nucleus nor too far from the nucleus. Close to the

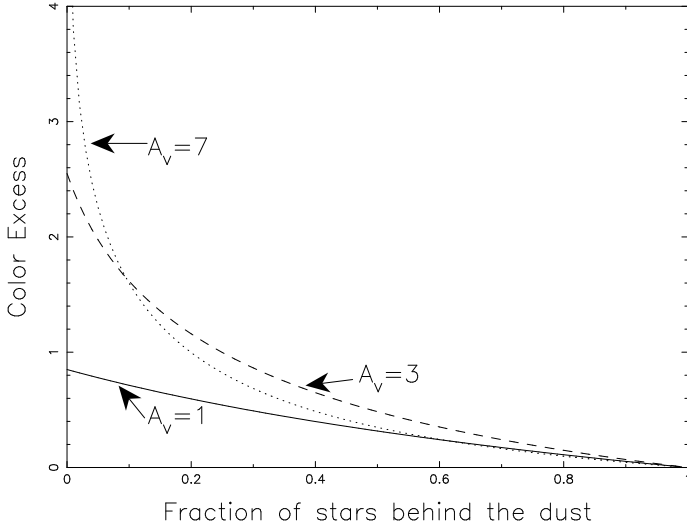


Fig. 3.— A plot of the color excess for a thin sheet of dust embedded in plane of stars. The solid line, dashed line, and dotted line represent an optical depth in V-band of 1, 3, and 5 magnitudes respectively. The color excess is calculated using a V–H color which is a close match to the F606W–F160W color used in the paper. Notice how if the most of the dust is in the mid-plane of the galaxy there is a maximum color excess of 0.6 magnitudes.

nucleus the inclination of the disk does not result in enough change in the z height of the disk to affect the amount of bulge stars seen in the background. Far from the nucleus the contribution of bulge stars to the total light is not high enough to significantly affect the colors. If these very red colors are due to a projection effect then they should be: only on one side of the galaxy, within the bulge region, and not too close to the nucleus. This projection effect may explain the color excesses in NGC 1241, NGC 3081, NGC 3516, and NGC 5347. It cannot explain the other galaxies and most importantly the three galaxies with the highest color excesses (Mkn 1066, NGC 6300, and NGC 7582) do not fit this view. Mkn 1066 and NGC 7582 have very high color excesses on opposite sides of the nucleus. A disk inside a bulge cannot produce high color excesses on different sides of the galaxy. In NGC 6300 the peak color excess is less than $0''.15$ (< 10 pc) from the nucleus. This is too close for the projection effect to affect the color excess.

This leaves the possibility that the scale height of the dust is higher than the scale height of the stars. In NGC 6300 not only must the scale height of the dust be very high but the dust needs to be mostly in front of the galaxy.

6. Conclusions

Our color maps reveal a nuclear dust morphology that is not consistent with strongly barred potentials being the only or even the primary mechanism of driving gas into the nuclear region. Only three of the 12 galaxies exhibit the straight dust lanes indicative of a strongly barred potential. Two of the galaxies have slightly curved dust lanes which could be caused by a weak bar or oval distortion. Our color maps allow us to recognize that what appear to be nuclear bars in our NICMOS images of Markarian 1066 and NGC 7582 are more likely regions of nuclear star formation. The lack of nuclear bars in these Seyfert galaxies implies that there are other mechanisms of fueling the nucleus or that Seyfert nuclei do not require continuous fueling to remain active.

Another fueling mechanism could be the spiral dust lanes that are quite common in our sample. Many of the dust lanes can be traced to approach the nucleus up to the limit of our resolution ($\sim 0''.15$). Mechanisms of both spiral arm formation and spiral arm fueling in the nuclear regions of galaxies need to be investigated.

We have shown how the dust morphology can be a sensitive probe of the gravitational potential in a galaxy. The lower velocity dispersion of the gas makes it respond much more readily to perturbations. In addition, using the dust morphology avoids the problems of stellar isophotes being affected by either dust extinction or current star formation.

Our color maps require that the dust in several of the galaxies be distributed relatively high compared to the stars. Only by putting the dust in front of most of the stars is it possible to achieve the amount of reddening that we observe. This high scale height dust is seen very near the nucleus of the galaxies where the scale of the stars is large.

The authors would like to acknowledge helpful discussions with Johan Knapen, Issac Shlosman, and Bruce Elmegreen and helpful comments from the referee. Support for this work was provided by NASA through the Hubble Fellowship grant #HF-01100.01-98A awarded by the Space Telescope Science Institute, which is operated by the Association of Universities for Research in Astronomy, Inc. for NASA under contract NAS 5-26555. Support for this work was also provided by NASA through grant number GO-07330 from the Space Telescope Science Institute, which is operated by the Association of Universities for Research in Astronomy, Inc. for NASA under contract NAS 5-26555.

REFERENCES

Alonso-Herrero, A., Ward, M. J., & Kotilainen, J. 1996, MNRAS, 278, 902

Athanassoula, E. 1992, MNRAS, 259, 345

Bruzual, A. G., Magris, G., & Calvet, N. 1998, ApJ, 333, 673

Caldwell, N., Rose, J. A., & Dendy, K. 1999, AJ, in press

Elmegreen, B. G., et al. 1998, ApJ, 503, 119L

Falcke, H., Wilson, A. S., Simpson, C. 1998, ApJ, 502, 199

Ho, L. C., Filippenko, A. V., & Sargent, L. W. 1997, ApJ, 487, 591

Kormendy, J. & Richstone, D. 1995, ARA&A, 33, 581

Lin, C. C. & Shu, F. H. 1964, ApJ, 140, 646

Piner, B. G., Stone, J. M., & Teuben, P. J. 1995, ApJ, 449, 508

Kotilainen, J. K., et al. 1992, MNRAS, 256, 125

Laine, S., Knapen, J. H., Perez-Ramirez, D., Doyon, R., & Nadeua, D. 1998, MNRAS, in press

McLeod, K. K. & Reike, G. H. 1995, ApJ, 454, 95

Malkan, M. A., Gorjian, V., & Tam, R. 1998, ApJS, 117, 25

Miller, B. W., Whitmore, B. C., Schweizer, F., & Fall, S. M. 1997, AJ, 114, 2381

Mirabel et al. 1999, A&A, 341, 667

Mulchaey, J. S. & Regan, M. W. 1997, ApJ, 482, 135L

Mulchaey, J. S., Regan, M. W., & Kundu, A. 1997, ApJS, 110, 299

Phillips, A. C., Illingworth, G. D., MacKenty, J. W., & Franx, M. 1996, AJ, 111, 1566

Pogge, R. W. & De Robertis, M. M. 1995, ApJ, 451, 585

Regan, M. W. & Vogel, S. N. 1995, ApJ, 21L

Shlosman, I., Frank, J., & Begelman, M. C. 1989, Nature, 338, 45

Thornley, M. D. & Mundy, L. G. 1997, ApJ, 490, 682

Whitmore, B. C., Schweizer, F., Leitherer, C., Borne, K., Robert, C. 1993, AJ, 106, 1354

Witt, A. N., Thronson, H. A., Jr., & Capuano, J. M., Jr. 1992, ApJ, 393, 611

Zitelli, V., Granato, G. L., Mandolesi, N., Wade, R., Danese, L. 1993, ApJS, 84, 185

Table 1. Galaxy Characteristics

Galaxy	R.A. J2000	Dec. J2000	Hubble Type	Systemic Velocity ^a	Linear Scale
Markarian 573	01 ^h 43 ^m 57 ^s .8	02°21'00"0	SAB(rs)0+ Sy2	5174 km s ⁻¹	350 pc arcsec ⁻¹
Markarian 1066	02 ^h 59 ^m 58 ^s .6	36°49'14"0	SB(s)0+ Sy2	3605 km s ⁻¹	240 pc arcsec ⁻¹
NGC 1241	03 ^h 11 ^m 14 ^s .7	-08°55'20"0	SB(rs)b Sy 2	4052 km s ⁻¹	270 pc arcsec ⁻¹
NGC 1667	04 ^h 48 ^m 37 ^s .1	-06°19'11"9	SAB(r)c Sy2	4547 km s ⁻¹	300 pc arcsec ⁻¹
NGC 3032	09 ^h 52 ^m 08 ^s .2	29°14'10"0	SAB(r)0	1533 km s ⁻¹	100 pc arcsec ⁻¹
NGC 3081	09 ^h 59 ^m 29 ^s .5	-22°49'35"0	SAB(r)0/a Sy2	2385 km s ⁻¹	160 pc arcsec ⁻¹
NGC 3516	11 ^h 06 ^m 47 ^s .5	72°34'06"9	SB(s)0 Sy1.5	2649 km s ⁻¹	180 pc arcsec ⁻¹
NGC 3982	11 ^h 56 ^m 28 ^s .1	55°07'31"0	SAB(r)b Sy2	1109 km s ⁻¹	75 pc arcsec ⁻¹
NGC 5347	13 ^h 53 ^m 17 ^s .8	33°29'27"0	SB(rs)ab Sy2	2335 km s ⁻¹	160 pc arcsec ⁻¹
NGC 6300	17 ^h 16 ^m 59 ^s .2	-62°49'11"0	SB(rs)b Sy2	1110 km s ⁻¹	75 pc arcsec ⁻¹
NGC 7582	23 ^h 18 ^m 23 ^s .5	-42°22'14"1	SB(s)ab Sy2	1575 km s ⁻¹	105 pc arcsec ⁻¹
NGC 7743	23 ^h 44 ^m 21 ^s .5	09°56'04"5	SB(s)0+ Sy2	1710 km s ⁻¹	115 pc arcsec ⁻¹

^aAll velocities in this table use the optical convention

Table 2. Nuclear Dust Characteristics

Galaxy	Nuclear Dust Morphology	Maximum Color Excess
Markarian 573	spiral	0.3 mag
Markarian 1066	spiral	1.9 mag
NGC 1241	ring	1.1 mag
NGC 1667	spiral	0.9 mag
NGC 3032	spiral	0.6 mag
NGC 3081	bar	0.7 mag
NGC 3516	spiral	0.5 mag
NGC 3982	spiral	0.8 mag
NGC 5347	bar	0.9 mag
NGC 6300	amorphous	2.6 mag
NGC 7582	ring	2.7 mag
NGC 7743	bar	0.5 mag